J. Fluid Mech. (1996), vol. 320, pp. 139–161

Dissipation scale and control of fine-scale turbulence in a plane mixing layer

By YITSHAK ZOHAR[1] AND CHIH-MING HO[2]

[1]Department of Mechanical Engineering, The Hong Kong University of Science and Technology, Hong Kong

[2]Department of Mechanical and Aerospace Engineering, University of California, Los Angeles, Los Angeles, CA 90095, USA

(Received 9 December 1993 and in revised form 2 March 1996)

The entrainment of fluids from two streams into the shear region of an incompressible mixing layer is dominated by the evolution of large coherent structures. However, fine-scale mixing of the entrained fluids mainly occurs at the interfaces of the small-scale turbulence. In this investigation, experiments were conducted to understand the properties of the small scales and to explore a method for controlling the population of the fine-scale turbulence. Furthermore, a dissipation scale, ζ, is found from the zero-crossing of the time derivative of the velocity fluctuations. This scale characterizes the most probable size of fine-scale turbulence, which produces most of the viscous dissipation.

1. Introduction

In a mixing layer, the processes by which irrotational fluids in the two streams are engulfed into the shear region and attain vorticity have always been subjects of active research. Motion of the random small scales was traditionally thought to play a major role, and extensive statistical studies were carried out. About two decades ago, Brown & Roshko (1974) as well as Crow & Champagne (1971) recognized the existence of spanwise organized vortical structures and their dynamic importance. Later, another type of organized structure, streamwise vortices, was found (Konrad 1976). They are counter-rotating vortex pairs interlaced with spanwise structures (Bernal & Roshko 1986; Nygaard & Glezer 1991). The trend of research then shifted to investigate large quasi-periodic vortices. It is now well established that the mass transfer across the shear region of subsonic two-dimensional flows is accomplished by vortex coalescence (Winant & Browand 1974). In three-dimensional flows, the mass entrainment is produced by other types of unsteady evolution of the structures, such as the azimuthal deformation of asymmetric vortices (Ho & Gutmark 1987). These spanwise structures originate from Kelvin–Helmholtz instability waves. Since the instability is sensitive to the boundary conditions and the initial perturbations, the evolution of the structures can be manipulated by controlled disturbances (Ho & Huang 1982; Oster & Wygnanski 1982). For surveys of coherent structures research, one may consult Roshko (1976), Ho & Huerre (1984) and Wygnanski & Petersen (1987).

After the fluids have been entrained into the shear region by the evolving large vortices, complete mixing of the fluids needs a large interface area. This is provided

by the highly convoluted interface of the small scales. Thus, the fine-scale turbulence should be an inseparable part of turbulence research. Utilizing knowledge of coherent structures and advances in signal processing, we can study small-scale turbulence from a new perspective which is much more informative than the statistical approaches practised two decades ago. Following this thought, Huang & Ho (1990) investigated the fine-scale transition process by using the phase-averaging and the peak-valley-counting (PVC) techniques on the instantaneous velocity traces. In the Reynolds number range allowed by their facility, the transition was found to occur around the vortex-merging region, in the plane containing the cores of the streamwise vortices.

Theoretically, Liu (1981) demonstrated that a significant amount of energy was transferred from the mean flow to the fine scales where the growth of the large-scale structures reached maximum. Using a high-resolution computation domain, Rogers & Moser (1992) and Moser & Rogers (1993) computed the mixing layer through transition. They also detected that small eddies first appear in the cores of the spanwise structures and in the plane containing the core of the streamwise vortices.

In an acid–base reacting flow, Breidenthal (1981) investigated the mixing process. He showed that the mixedness, representing the degree of mixing, rose fast with the downstream distance and reached an asymptotic value. When the streamwise coordinate was normalized by the velocity ratio and the initial instability wavelength, the rise in mixedness (figure 13 in Ho & Huerre 1984) was found to also occur around the vortex-merging region where the flow becomes turbulent. This suggests that the mixing transition coincides with the small-scale transition. Indeed, it is expected since the large number of fine scales provides the interfaces for mixing.

In this paper, we first identify a length scale based on the extrema of the velocity fluctuations and then determine the scaling for the strain rate produced by the fine eddies. Last, a control technique is found to increase the amount of small-scale turbulence in the flow.

2. Experimental arrangement

2.1. *Wind tunnel*

The experiments were conducted in an open loop wind tunnel located at the fluid mechanics laboratory of the University of Southern California. Air is drawn through the tunnel by a suction fan downstream of the test section. Four turbulence-damping screens span the entire stilling chamber downstream of a honeycomb panel. The splitter plate was constructed in sections and carefully sealed against each screen. It tapers uniformly through the contraction section with an angle of 2°. At the end of the contraction section, a steel plate is attached to the end of the splitter plate to divide the test section into two streams, each 30.5 cm deep and 91.4 cm wide. The splitter plate tapers only on the low-speed side and terminates with an edge about 0.5 mm thick. In order to obtain different velocity ratios between the lower and upper streams, a series of cloth meshes was placed over the upper entrance to the stilling chamber to produce an increased pressure drop and, subsequently, a velocity difference at the plate trailing edge.

A traversing mechanism is housed in a large Plexiglas compartment resting on the roof of the tunnel. Probes are mounted on a traverse and are introduced into the test section through the low-speed stream. DC stepping motors drive lead screws in the traverse to move the probe in all three directions.

2.2. *Forcing technique*

Acoustic waves were applied to force the mixing layer using a speaker array developed by Professor F. K. Browand at USC. A row of 17 speakers span the tunnel ceiling directly above the trailing edge of the splitter plate. The speakers are housed in a Plexiglas compartment lined with foam to damp acoustic reflections. The speakers are driven by individual power amplifiers which are fed by a common signal source. The driving signal is provided by an electronic device which can generate a sine wave of a desired frequency along with its subharmonics. The perturbation to the flow can then be a single fundamental frequency or up to three combined frequencies – the fundamental with its first and second subharmonics. The amplitude and the phase shift of each component signal can be controlled. The acoustic field generated by this array of speakers was uniform across the span to within 5 dB, as measured by a microphone at the trailing edge.

2.3. *Instrumentation and data reduction*

A single hot wire was used to determine the mean and fluctuating longitudinal velocity. The wire used for small-scale detection was made of 10% rhodium–platinum, 2.5 μm in diameter and about 0.5 mm in length. The wire used for recording the passage of the large scales, providing the phase reference, was made of platinum, 2.5 μm in diameter and about 1 mm in length. The constant-temperature anemometer had a flat frequency response up to 30 KHz. The hot-wire output voltage was calibrated against a Pitot tube. A fourth-degree polynomial fit was used with the five required coefficients determined by using a least-squares algorithm.

The analog output of the wires was digitized with a PC-based data acquisition system; its fastest digitizing rate is 1 MHz. The actual digitizing time used in this experiment was 6 μs, yielding an acquisition rate of about one order of magnitude higher than the most-probable frequency of the small-scale structures. A fast-Fourier-transform (FFT) algorithm was used to compute frequency spectra for the streamwise velocity, and the one-dimentional spectra in wavenumber space was obtained by assuming Taylor's hypothesis, $k_x = 2\pi f/U_c$. The latter spectra were corrected for wire resolution, following the procedure described by Wyngaard (1968), and then smoothed using a spline algorithm. The three-dimensional energy spectra as well as the dissipation spectra were obtained from the one-dimentional spectra by assuming isotropic relationships as shown by Wyngaard (1968). The reference signal was filtered using an FIR digital filter to remove contributions from small scales, enabling easier detection of the zero crossings. Thus, a clear phase reference for the passage of the coherent structures was provided, which is needed for conditional averaging.

The peak–valley-counting (PVC) technique was used to detect the small-scale structures; a schematic illustration of the method is shown in figure 1. The technique was developed by Huang (1985) and Hsiao (1985), and its algorithm was further improved by Zohar (1990). The basic idea of this scheme is to mark every local velocity maximum and local velocity minimum for further signal processing. First, the d.c. component is removed to increase the resolution for examining the velocity fluctuations. Then the local velocity maxima (peak) and minima (valley) are determined. The time separation between a peak–valley pair, Δt, is related to a small-scale event, and the velocity difference corresponding to the two instants is denoted by Δu. The time difference between each pair of successive positive zero crossings, T_i, represents the passage of a large-scale structure. The separation between a positive zero crossing and a small-scale event, t_i, marks the instant of occurrence of small-scale turbulence within the large-scale structure and is used for phase-averaging analysis.

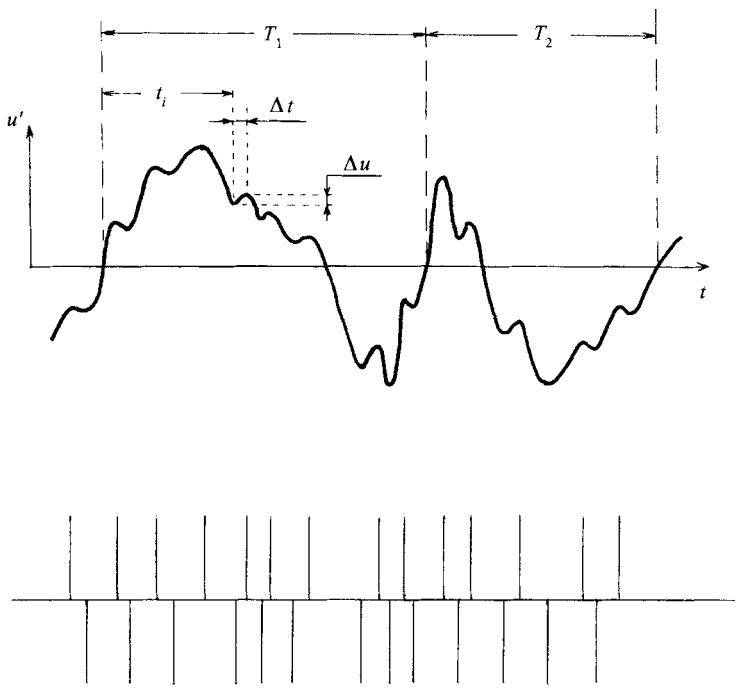

FIGURE 1. Schematic illustration of the PVC technique.

3. Time-averaged flow field of the mixing layer

3.1. *Initial conditions*

All experiments were conducted with laminar boundary layers on both sides of the splitter plate. Evidence for the laminar state of the boundary layers at separation was obtained from traverses across the flow at $x = 0.25$ mm downstream of the plate trailing edge. Figure 2 compares the mean velocity distributions on both sides of the plate with the Blasius profile for the highest speed used for either stream. Energy spectra showed wide-band background noise with no preferred component (Zohar 1990). The free-stream flow was uniform across the span to within 0.35% of the maximum velocity in either stream. The turbulence level in the vicinity of the trailing edge was approximately 0.3% .

Most experiments were performed with free-stream velocities $U_1 = 2.75$ m s^{-1} and $U_2 = 12.65$ m s^{-1}, so the velocity ratio was $R = (U_2 - U_1)/(U_2 + U_1) = \Delta U/2\overline{U} = 0.64$. Based on the initial velocity profile with a wake defect, the initial vorticity thickness as determined by the method proposed by Zhang, Ho & Monkewitz (1985) was $\delta_{\omega 0} = 3$ mm, and the Reynolds number was $R_e = \overline{U}\delta_{\omega 0}/\nu = 1540$. The initial instability frequency was found to be $f_0 = 380$ Hz, which corresponds to the Strouhal number of $S_{t0} = f_0\delta_{\omega_0}/\overline{U} = 0.148$, close to the value of 0.136 predicted by Monkewitz & Huerre (1982) for $R = 0.7$.

3.2. *Length scales*

Near the origin of the mixing layer, the Kelvin–Helmholtz instability waves grow with downstream distance and possess a preferred wavelength which is $\Lambda_0 = \overline{U}/f_0 =$ 20 mm. The streamwise coordinate is normalized by the velocity ratio and the initial instability wavelength, $X = Rx/\Lambda_0$, following the scaling rule suggested by Ho & Huang (1982). Based on this scaling, the first and second vortex mergers occur

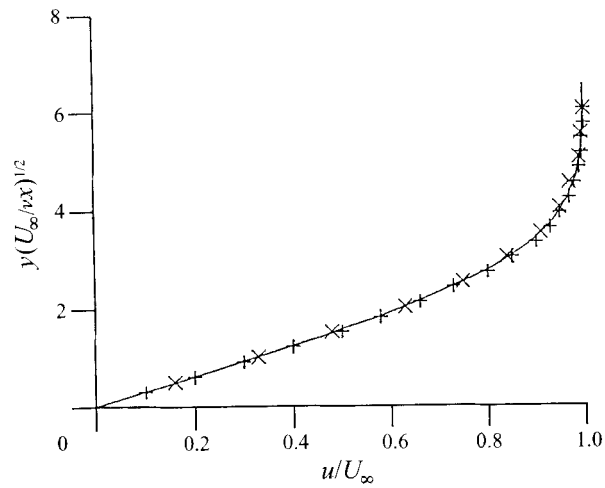

FIGURE 2. Boundary layer velocity profiles: +, $U_1 = 6$ m s^{-1}; ×, $U_1 = 24$ m s^{-1}; ——, Blasius profile.

at $X = 4$ and 8 respectively (Ho & Huerre 1984). As vortex merging goes on, the phase de-correlation phenomenon prevails (Ho *et al.* 1991), and the location of vortex merging jitters in space. The vortex passage frequency, f_x, decreases and wavelength, Λ_x, increases linearly with streamwise distance. The average local streamwise spacing of the spanwise vortices is $\Lambda_x = \overline{U}/f_x$.

Close to the trailing edge, the velocity profiles exhibit a wake-like defect. The wake disappears within one initial instability wavelength. The conventional vorticity thickness,

$$\delta_\omega \equiv \frac{U_2 - U_1}{(\partial U/\partial y)_{max}} \tag{3.1}$$

or the momentum thickness,

$$\theta \equiv \frac{1}{(\Delta U)^2} \int_{-\infty}^{\infty} (U_2 - \overline{U})(\overline{U} - U_1)\, \mathrm{d}y \tag{3.2}$$

can be used for the transverse length scale. The velocity profiles normalized by either θ or δ_ω reach self-similarity about six initial instability wavelengths, Λ_0, downstream from the splitter plate. In this paper, figure 3, local $\delta_\omega(x)$ is used for normalization, $Y = y/\delta_\omega(x)$.

The counter-rotating streamwise vortices, ribs, are stationary in the wind tunnel (Jimenez, Martinez-Val & Rebollo 1979). These vortices are associated with mixing of fluids from the high-speed side to the low-speed side and vice versa. This results in corrugated spanwise profiles of the averaged streamwise velocity (see figure 4) across the entire shear layer. This type of profile provides an easy way to determine the wavelength of the ribs. The spanwise wavelengths, Λ_z, increases with streamwise distance. The ratio between the local spanwise and streamwise wavelengths is independent of x, about 0.6, in agreement with the value found by Huang & Ho (1990) as well as Pierrehumbert & Widnall (1982). This spanwise wavelength is used to normalize the spanwise coordinate, $Z = z/\Lambda_z(x)$.

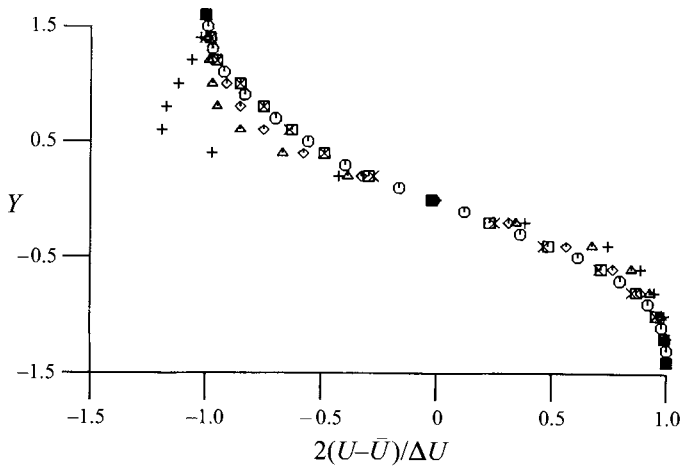

FIGURE 3. Transverse velocity profiles, $U(y)$:
+, $X = 1$; △, $X = 2$; •, $X = 4$; ×, $X = 6$; $X = 8$; ○, $X = 10$.

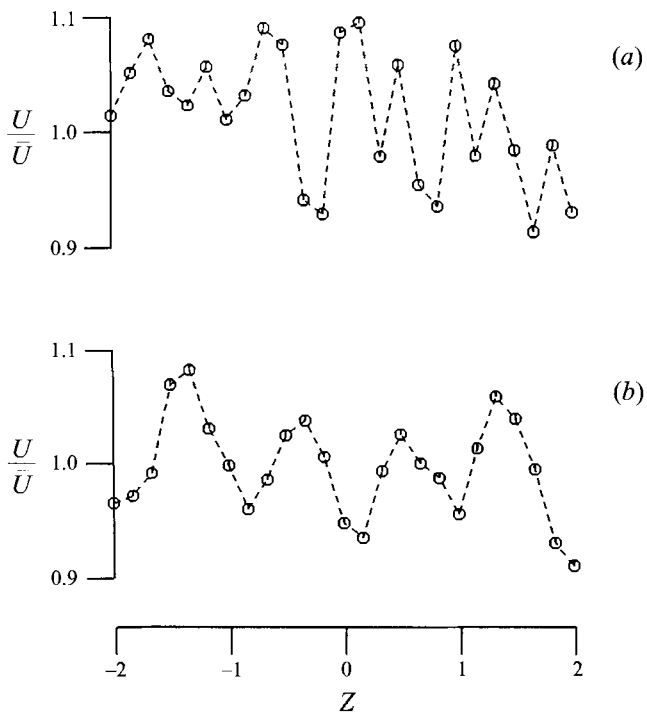

FIGURE 4. Spanwise velocity profiles, $U(z)$: (*a*) $X = 4$; (*b*) $X = 8$.

4. Spatial distribution of the fine scales

An initially laminar mixing layer will undergo transition to a turbulent flow. The turbulent region is characterized by very active small-scale turbulence in the shear layer. In the Reynolds number range of the present wind tunnel, the small scales start to appear downstream of the first vortex merging, $X = 4$. By the second vortex merging, $X = 8$, they have nearly reached an asymptotic state. The physical properties, distribution and evolution of these small eddies will be presented here.

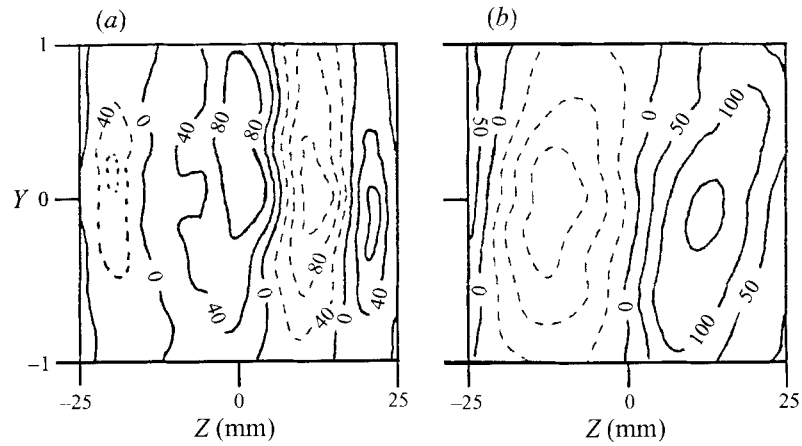

FIGURE 5. Contours of constant $\partial U/\partial z$ (s^{-1}) in the (Y,Z)-plane: (*a*) $X = 4$; (*b*) $X = 8$.

4.1. *Small-scale population in planes normal to the streamwise direction*

Huang & Ho (1990) reported that during the initial stage of the small-scale transition, fine scales are not uniformly distributed in the spanwise direction. They are more populous in the cores of the streamwise vortices. This finding was based on a few time traces of the velocity signals. In order to substantiate the finding, we surveyed the small-scale population distribution in the (y,z)-plane normal to the streamwise direction. Two planes were mapped with 11×11 stations each, one plane located at $X = 4$ and the other one at $X = 8$. Two hot wires were used for the measurement. One was the sampling probe for velocity fluctuations. The other probe was situated at exactly the same spanwise station at the high-speed edge of the shear layer, $Y = -1$, and its signal recorded the passing phase of the coherent structures. The output of the second probe was used as a phase reference for phase averaging. The time record digitized at each station was equal to five hundred periods of the passing rollers. Each period was determined from a pair of successive zero crossings with positive slopes in the fluctuating signal of the reference wire. Data are first presented in the time-averaged form and then followed by the phase-averaged information denoted by $\langle\ \rangle$.

In this experiment, only the streamwise velocity was measured. Therefore, one part of the transverse vorticity component, $\partial U/\partial z$, was used to indicate the location of the streamwise vortices. The contours of constant time-averaged $\partial U/\partial z$ show the counter-rotating vortex pairs (figure 5). At $X = 4$, two pairs of vortices were observed in the measuring domain. But, at $X = 8$, only one vortex pair was detected in the same survey range, because the spanwise wavelength of the ribs doubles after vortex merging (Huang & Ho 1990). Bell & Mehta (1992) observed the same trend of doubling of the spanwise wavelength. In their experiment, the total streamwise vorticity was measured.

The time-averaged number of velocity maxima or minima found during one period of coherent structures is defined as the population density, $N(x,y,z)$. N is a measure of the average number of small scales contained in a typical coherent structure passing the measuring station. The time-averaged iso-contours of N in the (Y,Z)-plane are plotted for two streamwise stations in figure 6. At $X = 4$, there are two distinct peaks around $Z = 0.25$ where $N_max = 4$. These peaks coincide with the cores of the streamwise vortices (see figures 5*a* and 6*a*). At this streamwise location, random

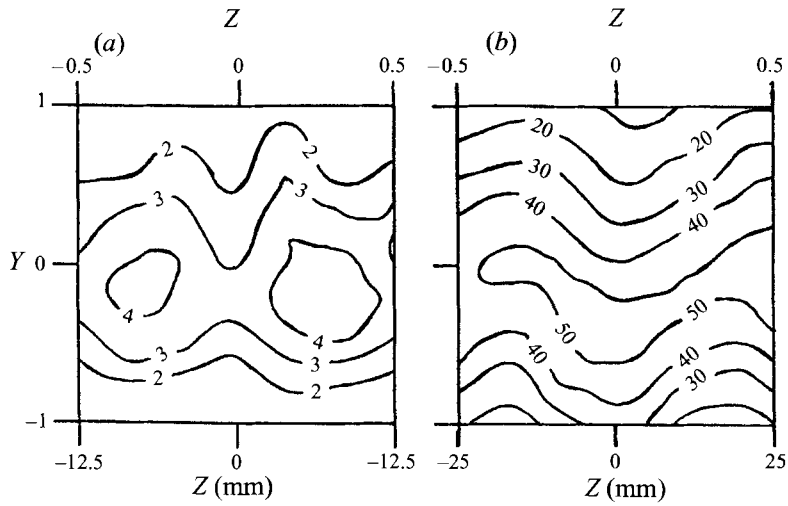

FIGURE 6. Contours of constant N in the (Y,Z)-plane: (*a*) $X = 4$; (*b*) $X = 8$.

fine-scale turbulence has not occurred yet. The measured small scales are the folds of the coherent structures. Further downstream, $X = 8$, the small-scale transition takes place and the peak value of N has increased by one order of magnitude to more than 50. The largest number of small scales in the cross-stream direction coincides with the maximum mean streamwise velocity shear, $(\partial U/\partial y)_max$. In the spanwise direction, contours of constant population density of small scales are modulated in the same way as the average velocity, $\overline{U}$. The modulation is due to the presence of the streamwise vortices.

With phase-averaging and PVC techniques, we can examine the phase-averaged population, $\langle N \rangle$, of small scales at a cut in relation to the passing spanwise structures. Figure 7 shows the iso-contours of $\langle N \rangle$ in a (y,z)-plane along the core of a roller (figure 7*b*,*d*) and along the braid between rollers (figure 7*a*,*c*). The value of phase-averaged population, $\langle N \rangle$, is not an intrinsic number, because it is equal to the time-averaged value of N divided by the number of bins used in the phase average. The number of bins is chosen to be eight in this experiment. Evidently, at both streamwise stations, $X = 4$ and 8, the population of small scales along the core of the rollers (figure 7*b*,*d*) is higher than that across the braid (figure 7*a*,*c*). In each cross-section, the pattern of the small-scale population resembles the pattern obtained for the time-averaged values (figure 6).

Around the first vortex merging the number of occurrences of fine-scale turbulence found inside a roller or a rib core is twice as large as that found between the cores. Recent numerical simulations by Moser & Rogers (1993) agree with this finding. Near the second vortex merging, around the end of the small-scale transition, the fine-scale turbulence spreads around the entire roller and does not concentrate only in the cores of the ribs.

4.2. *Small-scale population in planes normal to the spanwise direction*

By assuming Taylor's hypothesis, the pseudo-streamwise coordinate can be represented by multiplying the time with a convection speed. Here, $\overline{U}$ is taken as the convection speed. Each period represents a wavelength of one roller, Λ_x. Therefore, the normalized streamwise distance, $\langle X \rangle = \overline{U}t/\Lambda_x$, is between 0 and 1.

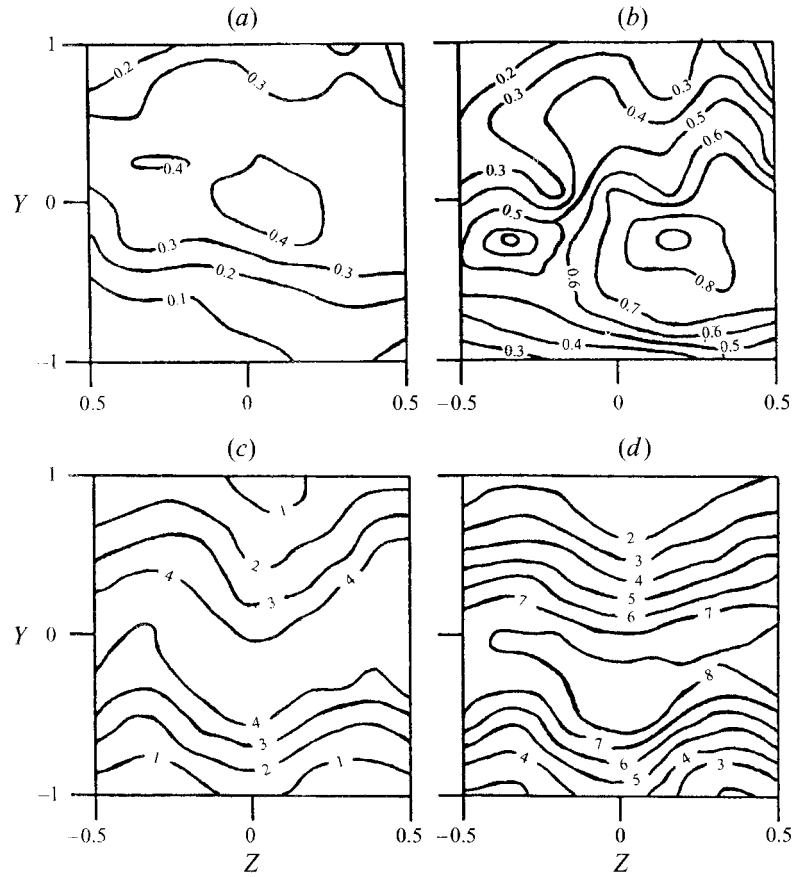

FIGURE 7. Contours of constant $\langle N \rangle$ in the (Y,Z)-plane: (*a*) $X = 4$, between rollers; (*b*) $X = 4$, roller plane; (*c*) $X = 8$, between rollers; (*d*) $X = 8$, roller plane.

The rollers are structures of coherent spanwise vorticity which has two components, $\omega_z = \partial v/\partial x - \partial u/\partial y$. Again, only the component containing the streamwise velocity, $\partial u/\partial y$, was used to indicate the structure. The phase-averaged streamwise velocity, $\langle u \rangle$, in the plane containing the core of the rib, $Z = 0.25$, was obtained at $X = 8$. Figure 8(*a*) shows the iso-contours of $\partial\langle u \rangle/\partial y$. The identities of the individual rollers are smeared out at the second vortex merging location, $X = 8$, and only the resulting core is noticeable around $\langle X \rangle = 0.5$. The phase-averaged streamwise derivative of u, $\partial\langle u \rangle/\partial x$, is the component of the strain-rate field induced by the roller shown in figure 8(*b*). The pattern obtained here is very similar to the strain rate of a single vortex. The centre of the core is a saddle point with antisymmetric strain-rate field in the four quadrants.

The phase-averaged small-scale population density in the roller is shown in figure 8(*c*). The largest number of small scales in the (x,y)-plane is found around the core of the roller where the spanwise vorticity is maximum corresponding to the saddle point in the $\partial\langle u \rangle/\partial x$ field. The PVC technique registers the local velocity extrema, u_h and u_l, and the instants, t_h and t_l, correspondingly. Hence, an estimation of the strain rate produced by the small-scale turbulence,

$$\frac{\Delta u}{\Delta x} \equiv \frac{u_h - u_l}{\overline{U}(t_h - t_l)}, \tag{4.1}$$

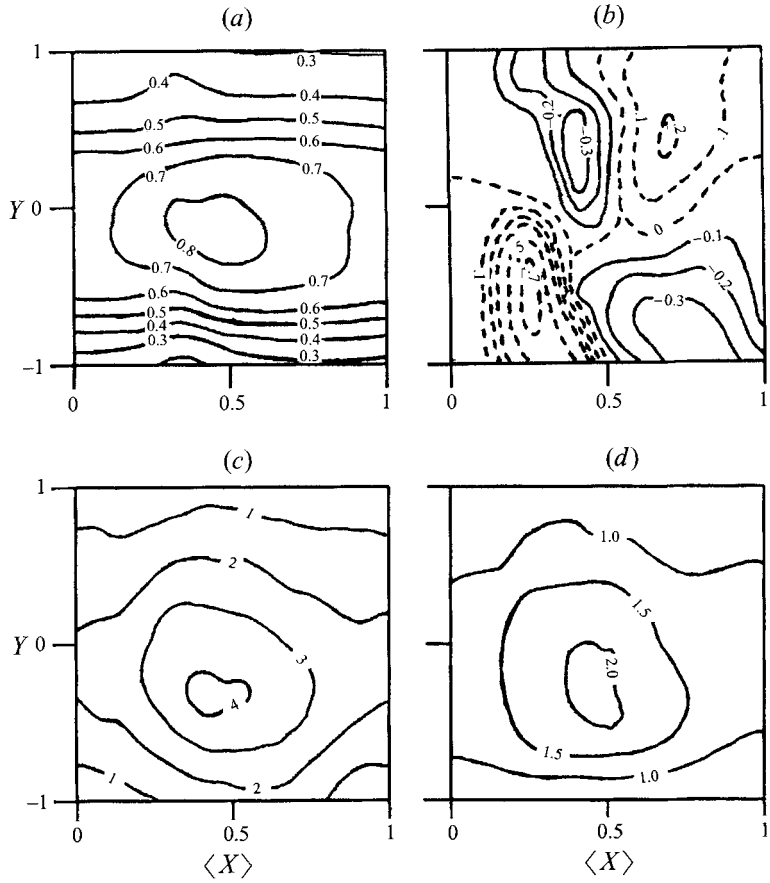

FIGURE 8. Contours in the (X, Y)-plane at $X = 8$ of constant: (*a*) $(\partial\langle u\rangle/\partial y)/(\Delta U/\Lambda_0)$; (*b*) $(\partial\langle u\rangle/\partial x)/0.1(\Delta U/\Lambda_0)$; (*c*) $\langle N\rangle$; (*d*) $(\Delta\langle u\rangle/\Delta x)/(\Delta U/\Lambda_0)$. $\Delta U/\Lambda_0 = 445$ (s^{-1}).

can be obtained. It should be noted that this quantity is not the true strain rate, $\partial u/\partial x$, which consists of the strain rate contributed by both the large and the small scales. The constant contours of $\Delta u/\Delta x$, figure 8(*d*), show that the highest-value is located at the same region as the high concentration of small scales, $\langle N\rangle$. If the small scales are approximately isotropic, the level of $\Delta u/\Delta x$ is an indication of the dissipation rate. Hence, it is expected that contours of $\langle N\rangle$ and $\Delta u/\Delta x$ exhibit similar spatial distribution.

4.3. *Streamwise variation of small-scale population*

Along the streamwise direction, the population of the small-scale turbulence must increase while the flow changes from a laminar to a turbulent state and eventually becomes a fully developed turbulent flow. The population density was measured with a hot wire traversed in the streamwise direction at $Z = 0$ and at Y where $U = \overline{U}$. Since the passage frequency, f_x, decreases with x, the duration of signal sampling, T_d, was increased with x such that $T_d = 500/f_x$. Therefore, five hundred rollers were sampled at each streamwise station. The number of small scales passing the hot wire during T_d was obtained by the PVC technique. The ratio between the number of small scales and the number of local passing rollers, N, is plotted in figure 9. The value increases sharply downstream from $X = 4$ due to transition and then increases

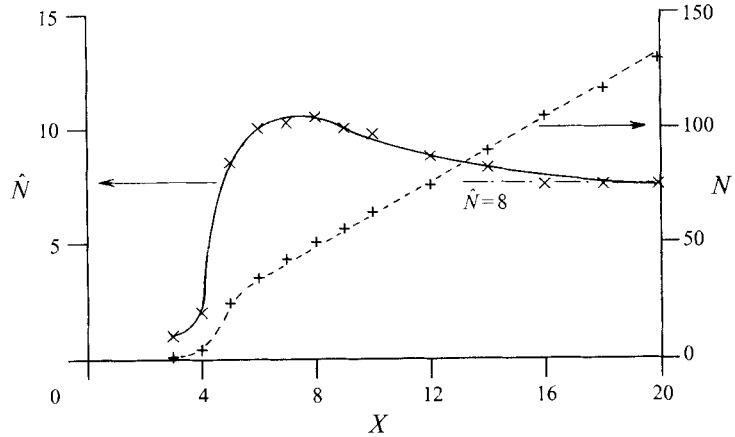

FIGURE 9. Streamwise evolution of small-scale population: —×—, $\hat{N}$; ---+---, N.

linearly with x. Hence, the amount of small-scale turbulence per large coherent structure increases with streamwise direction.

A time scale which is independent of the streamwise distance is the period of the initial instability waves. The number of small scales accumulated during T_d is then normalized by the number of initial instability waves during the same duration. The resulting value, $\hat{N}$, is plotted in figure 9. An abrupt increase of $\hat{N}$ occurs downstream of $X = 4$ and it reaches a maximum around $X = 8$. Further downstream, the values of $\hat{N}$ decrease very slowly. It implies that the size of the small-scale turbulence does not change significantly with x. In other words, the linear increase of N is mainly due to the increasing size of the coherent structures rather than the decreasing size of the fine-scale eddies.

5. A dissipation scale of the fine-scale turbulence

5.1. *Length scales of fine-scale turbulence*

In turbulence research, two microscales, the Kolmogorov scale and the Taylor scale, are used to characterize the size of fine-scale eddies producing viscous dissipation. The Kolmogorov scale is defined as

$$\eta \equiv (\nu^3/\epsilon)^{1/4} \tag{5.1}$$

where ν is the kinematic viscosity and ϵ is the rate of dissipation. For a local isotropic flow (Tennekes & Lumley 1972),

$$\epsilon = 15\nu\overline{(\partial u'/\partial x)^2} \tag{5.2}$$

where u' is the streamwise fluctuating velocity. The Kolmogorov scale is considered to be the smallest scale in turbulent flows.

From correlation of velocity fluctuations, an osculating parabola can be matched to the correlation curve at its origin. The distance between the origin and the intersecting point of the osculating parabola with the horizontal axis is defined as the Taylor microscale. Based on this definition the Taylor scale, λ, can be obtained as follows:

$$\lambda^2 \equiv (u^*)^2/\overline{(\partial u'/\partial x)^2} \tag{5.3}$$

where u^* is the r.m.s. value of the fluctuating streamwise velocity, u'.

The high-frequency velocity fluctuations (see figure 1) are caused by the fine-scale

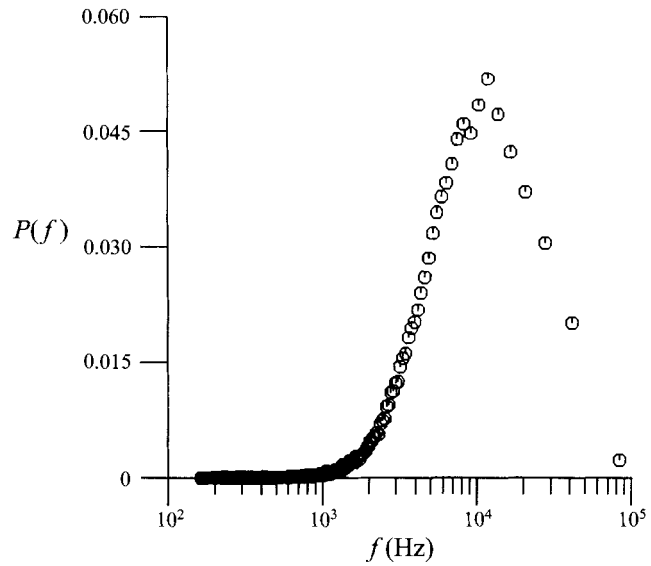

FIGURE 10. Frequency histogram of fine eddies at $X = 8$.

turbulence. The PVC technique registers the duration, Δt, of these fluctuations. These durations represent a direct measure of the time scales of the eddies passing the sampling probe. We then examine the histogram of the values of Δt. More than 10 000 of such events were used to produce the histogram. If the histogram is flat, it shows that the fine-scale turbulence has a wide distribution without a characteristic time scale. On the other hand, if a peak can be detected in the histogram, it means that small-scale turbulence has a preferred scale. Indeed, it is interesting to find out that we do observe a pronounced peak around 12 000 Hz in the histogram shown in figure 10. A length scale, ζ, is defined by multiplying the time scale located at the peak, $(f_p)^{-1}$, with the convection velocity, $\overline{U}$,

$$\zeta \equiv \overline{U}/f_p. \tag{5.4}$$

Here, f_p is the peak frequency where $\mathrm{d}P(f)/\mathrm{d}f = 0$. The convective velocity at this point in the flow field is 7.7 m s^{-1}. Thus, the length-scale value is $\zeta = 0.65$ mm, while the local streamwise wavelength is 80 mm. So at this location ($X = 8$, $Y = 0$ and $Z = 0.25$), this scale for the small eddies is about two orders of magnitude smaller than the scale of the rollers, indicating large separation between the scales of the small and the large eddies.

The value of the Kolmogorov scale at $X = 8$, $Y = 0$ and $Z = 0.25$ is 0.062 mm, as obtained from (5.1). The Taylor scale calculated from (5.3) at this location is 2.2 mm. So, the microscale ζ is about one order of magnitude larger than the Kolmogorov microscale and about 3.5 times smaller than the Taylor microscale.

5.2. *The spatial evolution of the microscale* ζ

In a mixing layer, the Reynolds number increases with the streamwise distance. The dependence of ζ on Reynolds number is examined as a function of the streamwise coordinate. The value of ζ increases with x at a very slow rate as shown in figure 11. The length scale of the large vortices, Λ_x, is a linear function of x and increases at a much faster rate than ζ. The Kolmogorov and Taylor microscales are determined

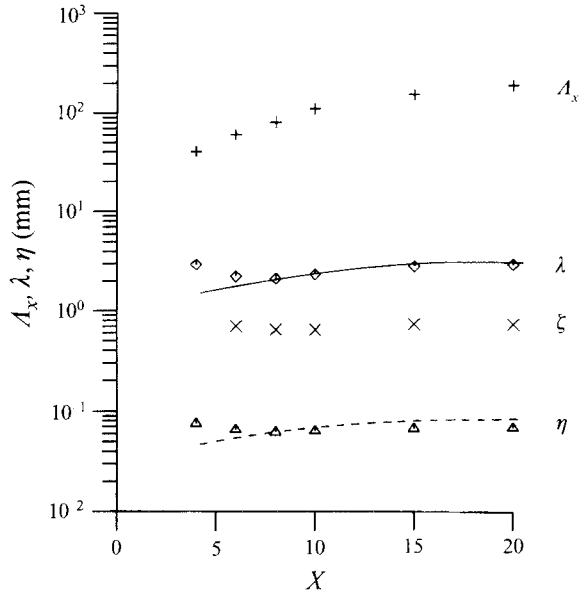

FIGURE 11. Streamwise evolution of the length scales: +, Λ_x; ◇, λ from (5.3); ——, λ from (5.6); ×, ζ; △, η from (5.1); – – – – –, η from (5.5).

in two ways. The values directly obtained from the definitions, (5.1) and (5.3), are plotted in figure 11. The separation between these three microscales is obvious. Both Kolmogorov and Taylor scales also grow slowly with the streamwise coordinate. The other way of estimating these two scales is from the relations between the microscales and the large scale,

$$\frac{\eta}{\Lambda_x} = \left(\frac{1}{A}\right)^{1/4} \left(\frac{u^* \Lambda_x}{\nu}\right)^{-3/4}, \tag{5.5}$$

$$\frac{\lambda}{\Lambda_x} = \left(\frac{15}{A}\right)^{1/2} \left(\frac{u^* \Lambda_x}{\nu}\right)^{-1/2}. \tag{5.6}$$

A is a constant and is about one. Equations (5.5) and (5.6) are valid under the assumption of local isotropy (Tennekes & Lumley 1972). These values match the data obtained from (5.1) and (5.3) very well downstream from $X = 8$. This is supporting evidence for the local isotropy assumption.

The functional relationship between ζ and the other two scales, or its dependence on Re_Λ is an interesting question. Within the Reynolds number range obtainable in this facility, the ratio ζ/η is about 10. The other ratio, ζ/λ, is not a constant. The reliability of the result is limited by the range of the Reynolds number based on a microscale, say Re_Λ. In most of the low-speed facilities, the Reynolds number based on the integral scale can be varied by about one order of magnitude, but it is only factor of three for the Reynolds number based on the Taylor microscale. The exact proportionality between ζ and η remains to be determined by more tests when a wider range of Re_Λ becomes achievable.

The variation of the microscale, ζ, in the cross-stream direction, y, is shown in figure 12. The data were taken at $X = 8$ and $Z = 0.25$. Within the shear region, $y/\delta_\omega \leqslant \pm 0.5$, the value of ζ is practically constant. At the end of the small-scale transition, the small-scale turbulence is fairly homogeneous inside the shear layer.

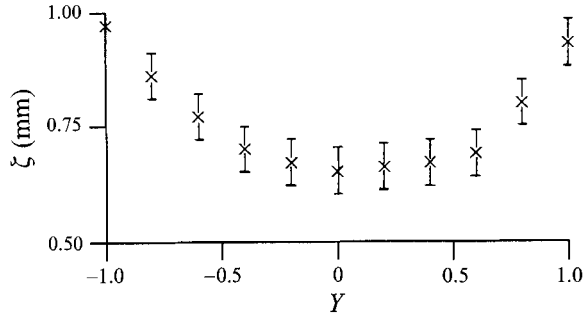

FIGURE 12. The transverse distribution of the microscale ζ.

However, at the outer region of the mixing layer, $y/\delta_\omega < -0.5$ and $y/\delta_\omega > 0.5$, the interfaces of the large coherent structures start to contribute to the velocity traces analysed by the PVC technique. Hence, the apparent size of the eddies increases at the outer edges of the shear region.

5.3. *Viscous dissipation*

The Reynolds numbers based on microscales are very small, and viscous effects are dominant in this range. Hence, Kolmogorov and Taylor microscales have always been associated with energy dissipation. We would therefore like to identify the role of the microscale, ζ, in the viscous dissipation.

The dissipation spectrum, $D(k)$, can be obtained from the three-dimensional energy spectrum, $E(k)$, as follows:

$$D(k) = k^2 E(k). \tag{5.7}$$

The three-dimensional energy spectrum was obtained from the measured streamwise velocity component, $u(t)$, following the procedure described by Wyngaard (1968). In Wyngaard's analysis, local isotropy is assumed. In the fully developed region, the fluctuating levels of the three velocity components show the isotropic property, $u^* \approx v^* \approx w^*$, (Wygnanski & Fiedler 1970). In the same facility as the present experiment, Huang & Ho (1990) showed that the fluctuation levels of the three velocity components are about the same downstream from the small-scale transition region, $X = 8$. Both spectra, energy and dissipation, obtained at $X = 8$ and $Y = 0$ are shown in figure 13. The Reynolds number based on the Taylor scale at this station is $Re_\lambda = \lambda u^*/\nu = 310$. At $X = 8$, the roll-off exponent of the spectrum reaches $-5/3$ (Huang & Ho 1990). It indicates the existence of a well-established inertial subrange which is a necessary, though not sufficient, condition for local isotropy. Furthermore, the separation between the peaks of the two spectra, see figure 13, is about two orders of magnitude, which provides more support for assuming local isotropy.

When the values of the Kolmogorov and Taylor microscales are indicated on the wavenumber axis, k, the Kolmogorov scale appears at the far end of the dissipation spectrum. This follows the definition of the Kolmogorov scale which represents the smallest eddies surviving from the viscous dissipation. The Taylor scale appears on the other side of the dissipation peak. These two observations are consistent in spectra measured at other spatial locations. Neither of these two scales coincides with the peak of the dissipation spectrum, k_p; k_p identifies the size of the fine eddies which are responsible for most of the viscous dissipation. An interesting point can be observed when the microscale ζ is indicated in figure 13. ζ is the scale which does coincide with the peak of the dissipation spectrum. In other words, *the new microscale, ζ, is*

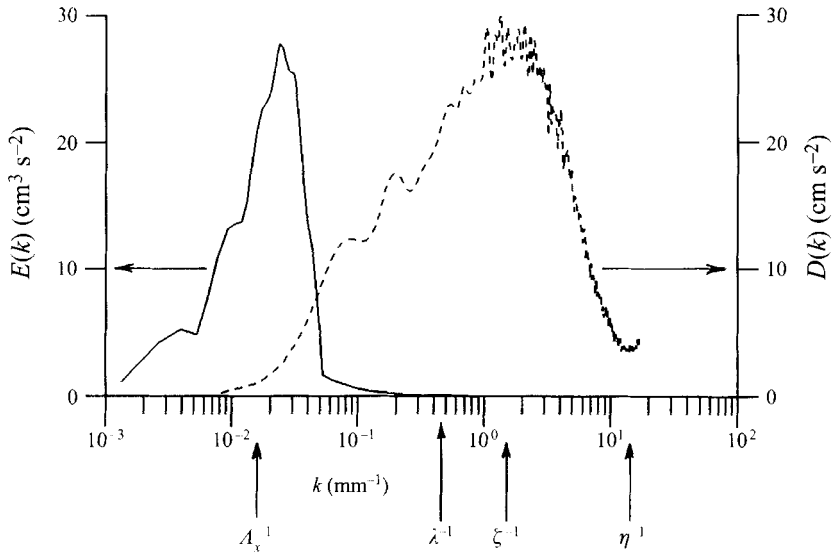

FIGURE 13. Dissipation spectra and the new dissipation scale, ζ: ——, energy spectrum; – – – – –, dissipation spectrum.

the typical length scale of small eddies producing energy dissipation. This result is not really surprising, if we review the way of determining the value of ζ: it represents the length scale of the most probable eddies (figure 10) defined from the local velocity extrema, $[U_c\Delta x]/[u_{max}-u_{min}]$. The value of $\Delta x/[u_{max}-u_{min}]$ to some extent represents the instantaneous velocity derivative which is related to the viscous dissipation ((4.1) and (5.2)).

In this study, only the streamwise velocity component was measured. In a study of a numerically simulated mixing layer (Zohar *et al.* 1990), all three velocity components were examined. The dissipation scales of the three velocity components are the same. In an experimental work by Foss (1994), all three velocity components were measured and the measured length scales confirm the numerical simulation result.

The relationship between the new microscale and the dissipation spectrum has been tested in other turbulent flows as well. Ho & Zohar (1996) investigated a plane mixing layer, a wake behind a cylinder and a plane boundary layer. Indeed, the microscale defined by the PVC histogram, ζ, was found to be equal to the scale of maximum dissipation in all three turbulent shear layers.

The physical meaning of the new dissipation scale, ζ, can be examined from energy balance considerations. The rate of the energy extracted by the large coherent structures from the mean flow is

$$\frac{\mathrm{d}E}{\mathrm{d}t} = \frac{\mathrm{d}}{\mathrm{d}t}(\tfrac{1}{2}u_iu_i) \approx \frac{(u^*)^2}{\Lambda_x/u^*} = \frac{(u^*)^3}{\Lambda_x} \tag{5.8}$$

and the viscous dissipation by the small scales is

$$\epsilon = \nu\frac{\partial u_i\partial u_i}{\partial x_j\partial x_j} \sim \nu\frac{(u^*)^2}{\Lambda_s^2}; \tag{5.9}$$

Λ_s is the length scale of small eddies. In a stationary turbulent flow, (5.8) should be

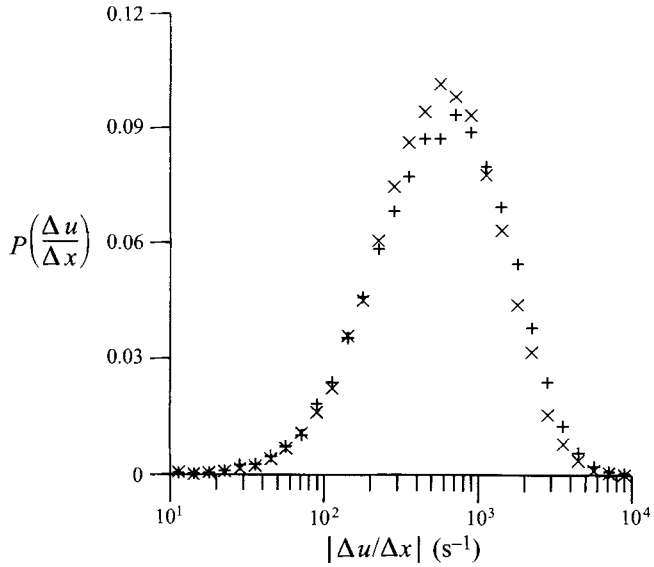

FIGURE 14. Histograms of the stretching and compression rate of fine eddies at $X = 8$: ×, $\Delta u/\Delta x > 0$; +, $\Delta u/\Delta x < 0$.

balanced by (5.9),

$$\frac{(u^*)^3}{\Lambda_x} = \nu \frac{(u^*)^2}{{\Lambda_s}^2}. \tag{5.10}$$

The r.m.s. of the streamwise velocity, u^*, and the roller wavelength, Λ_x, at the measuring location are 2.1 m s^{-1} and 8 cm respectively. The scale of the small eddies needed to maintain the energy balance is

$$\Lambda_s = (\nu \Lambda_x / u^*)^2 \tag{5.11}$$

and equals 0.75 mm which is very close to the value of $\zeta = 0.65$ mm. This is more evidence that ζ does represent the dissipation scale.

5.4. *Stretching or compression rate of fine-scale turbulence*

The quantity mentioned in the previous section, $[u_{max} - u_{min}]/\Delta x = \Delta u/\Delta x$, is a measure of the strain rate produced by small scales. However, one should be aware that it is not the conventional strain rate, $\partial u/\partial x$, which is a true derivative of velocity fluctuations and contains contributions from both large and small scales. The PVC technique biases the contribution of the small scales to $\Delta u/\Delta x$. Furthermore, $\Delta u/\Delta x$ is not a true derivative. When the value of $\Delta u/\Delta x$ is positive/negative, it represents the stretching/compression rate produced by small scales in Δx. When the probability density distributions (p.d.f.) of both the positive and the negative values of $\Delta u/\Delta x$ are plotted, figure 14, they exhibit pronounced peaks. This implies that the straining rate produced by the small scales has preferred values. Furthermore, the preferred stretching rate is the same as the preferred compression rate.

5.5. *Scaling of the small-scale properties*

The p.d.f. of Δx and the p.d.f. of $\Delta u/\Delta x$ have bell-shaped distributions. We can examine the joint p.d.f. in two dimensional space. The iso-contours of the joint p.d.f. at $X = 8$ and $Y = 0$ are shown in figure 15, where a single peak is evident. It has

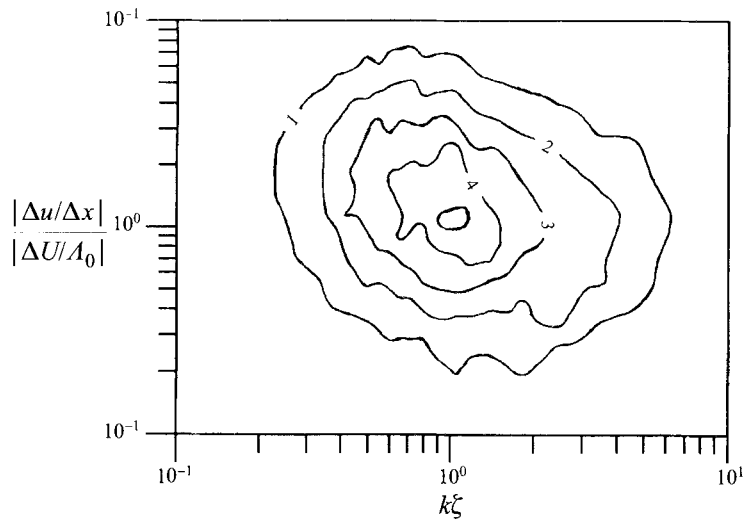

FIGURE 15. Joint histogram of fine-scale wavelength and strain rate at $X = 8$.

already been shown that the peak of the Δx-p.d.f. corresponds to the peak of the dissipation spectrum, k_p. Therefore, if the horizontal axis of figure 15 is normalized by k_p, the peak value should be one.

At this moment, the scaling of the vertical axis is not defined yet. If we use the velocity difference across the shear layer, ΔU, along with the initial instability wavelength, Λ_0, as the scaling parameters, the peak value of the normalized $\Delta u/\Delta x$ is also around unity. This is a very interesting result as it shows that *the most probable straining rate produced by the small scales equals the global straining rate produced by the mean shear.*

6. Control of finite-scale turbulence

The PVC technique developed here can identify individual fine-scale turbulence. In the previous sections, many different quantitative ways of examining small-scale turbulence activities, e.g. instantaneous information from the pulse train or the statistical quantities, have been demonstrated. This method allows us to precisely compare the small scales in a mixing layer under various operating conditions. For example, previous investigations have shown that a low level of forcing introduced at the trailing edge has a profound effect on the evolution of the organized structures in mixing layers (Ho & Huang 1982; Ho & Huerre 1984; Wygnanski & Petersen 1987). Whether fine-scale turbulence can be manipulated by active forcing is not known. Using the PVC technique to investigate the small-scale turbulence in natural and forced mixing layers can provide a definitive clue to the answer to this question. In this study, we have found that the two-dimensional forcing technique developed to control the spanwise rollers can also affect the production of small scales. In the case of influencing the evolution of the large structures, *low-level* perturbations can be effective. However, for the case of influencing the population of small scales, *high-level* subharmonic perturbations, of more than 100 dB acoustic intensity, are needed.

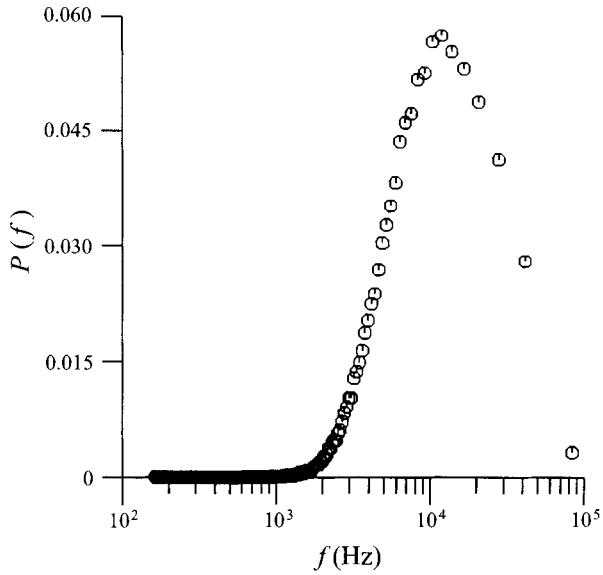

FIGURE 16. Frequency histogram of fine eddies for forced case at $X = 8$.

6.1. *Small-scale control by the fundamental frequency*

The flow was acoustically excited by an array of loudspeakers (§2.2). Hydrodynamic perturbations caused by the acoustic forcing are known to be small. As expected, the velocity fluctuations associated with the acoustic forcing at the trailing edge of the splitter plate are so low that no difference is observed between the forced and the natural power spectra (Zohar 1990). The velocity perturbations are within the background noise. We used the acoustic intensity output of the speakers as the reference for the forcing amplitude.

The histogram of fine scales determined by the PVC technique for the forced case at $X = 8$, $Y = 0$ and $Z = 0$ is shown in figure 16. The histogram has the same profile as the one obtained for the natural case (figure 10). The peak frequency is also at 12000 Hz. The most probable length scale, ζ, remains unchanged. This is not surprising because the size of the dissipation scale is determined by the Reynolds number and hence should not be affected by forcing. However, forcing does increase the amount of small-scale turbulence significantly. In each passing coherent structure, the small-scale population, N, increases from 50 in the natural case, to 70 in the forced case, at $X = 8$. Hence, the two-dimensional forcing not only affects the evolution of the coherent structures but also enhances the production of small scales.

In order to study the dependence of small-scale generation on the forcing level, the following experiment was conducted. The fundamental mode, $f_0 = 380$ Hz, was excited at four different levels, 100 dB, 110 dB, 120 dB and 130 dB. For each level, the maximum number of small eddies in a given cross-section was found. The same process was repeated for a number of streamwise stations. The range examined here extended from $X = 3$, where small eddies just start to appear, to $X = 20$, where the flow is expected to be fully developed. The number of small eddies normalized by the initial number of coherent structures, $\hat{N}$, is shown in figure 17. It indicates that between $X = 3$ and $X = 5$ the number of small eddies increased with the forcing level. However, $\hat{N}_{max} = 16$ seemed to be the saturation level. Attempts to increase this number by stronger forcing at the fundamental frequency yielded no higher number

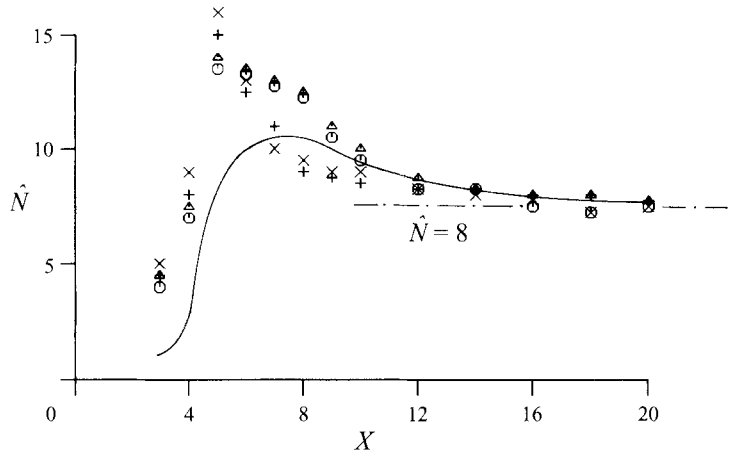

FIGURE 17. Effect of fundamental forcing level on fine-scale population: ○, 100 dB; △, 110 dB; +, 120 dB; ×, 130 dB; ——, natural.

than 16. For all levels of fundamental forcing the maximum value of $\hat{N}$ appeared at around $X = 5$. After the peak, the number of fine eddies decreased gradually to $\hat{N} = 8$ around the third vortex merging location, $X = 16$. Further downstream, all the curves collapsed onto a single one.

6.2. *Small-scale control by fundamental and subharmonic frequencies*

Two-dimensional forcing of a mixing layer has a limited range of influence along the streamwise direction. Exciting the fundamental mode alone leads to a phase locking of the roll-up process only. Adding the subharmonic to the forcing signal results in localizing the first merging process as well. Therefore, the zone of influence of the forcing can be extended by forcing fundamental and higher subharmonics, as successive vortex mergings become phase locked. Downstream from that location, phase de-correlation (Ho *et al.* 1991) will occur. The physical mechanism of the phase de-correlation is due to the detuning in the subharmonic resonance process.

The small-scale control experiment was repeated with the forcing signal a combination of the fundamental, $f_0 = 380$ Hz, and the subharmonic, $f_0/2 = 190$ Hz. Each component consisted of an amplitude equal to the highest fundamental forcing level, i.e. 130 dB. The results are compared in figure 18 with the unforced case and the case of forcing the fundamental frequency at the highest amplitude. It is obvious that each curve peaked at a different streamwise location. The zone of influence indeed depended on the frequency content of the perturbations. When the flow was forced at the fundamental only (§6.2), the peak of $\hat{N}$ occurred at $X = 4$, where the first vortex merging took place. The peak of $\hat{N}$ moved to the second vortex merging location, $X = 8$, for flow perturbed at fundamental and the first subharmonic. The zone of influence for the forced generation of small scales seemed to extend to the next vortex merging region compared with the phase de-correlation findings. This could have been due to the small-scale production in the present controlled case resulting from the interaction of the spanwise coherent structures which took place downstream from the phase-locked position of the spanwise structures.

The maximum value of $\hat{N}$ detected in both forced cases is 16, and is 1.5 times greater than the peak value for the natural case, $\hat{N}_{max} = 11$. This means that by forcing the shear layer, the small-scale population can be increased by as much as

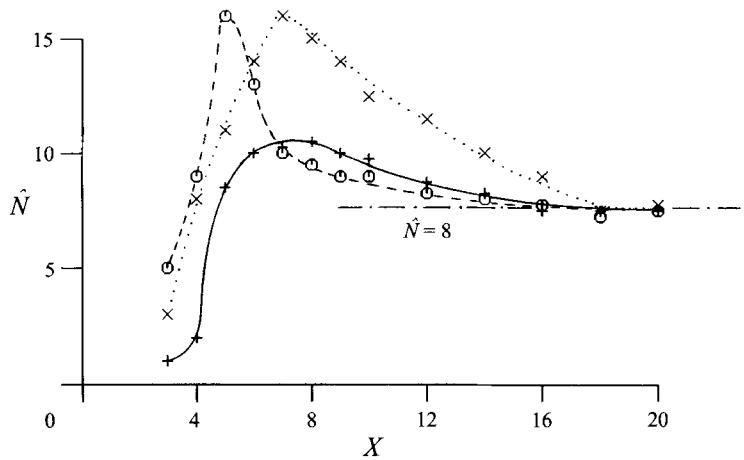

FIGURE 18. Effect of forcing on the evolution of fine-scale population: —+—, natural; ---o---, forced at f_0; ···×··· forced at $f_0 + f_0/2$.

50% relative to the unforced case. Moreover, it seems that the maximum value of $\hat{N}$ about 16, as it was obtained in all the tested forcing combinations. It is interesting to note that the ratio between the initial instability wavelength, $\Lambda_0 = 20$ mm, and the dissipation scale, $\zeta = 0.65$ mm, is about twice the peak value of 16. This suggests a simple explanation for the saturation value based on geometrical considerations. The initial instability wavelength, Λ_0, is dictated by the initial velocity profile. The scale of the small eddies, ζ, is dictated by the amount of energy to be dissipated, which is independent of forcing. Obviously, only a finite number of small eddies with a given length scale can be contained in the space occupied by a large eddy with a given size. Assuming that the small eddies are separated by a distance comparable to their size, the upper bound for $\hat{N}$ should be given by the ratio $\Lambda_0/2\zeta \approx 15.5$. Thus, the saturation level represents a state where the small eddies spread throughout the roller, beyond which their population cannot be further increased by forcing. Far downstream, the asymptotic level of small-eddy activity represents an equilibrium state to which the flow settles after the overshoot response in the transition region. The small-scale population, $\hat{N}$, attains an asymptotic value of 8. Since forcing has a limited zone of influence, it is expected that beyond that zone, the forced mixing layer will approach the unforced layer. Therefore, the asymptotic state should be independent of the forcing.

The distributions of the small-scale population in the plane normal to the streamwise direction (y, z-plane) are examined for the case forced by fundamental and subharmonic frequencies. The time-averaged number of small eddies contained in a local passing large eddy is shown in figure 19 for two stations, $X = 4$ and 8. The patterns are very similar to those obtained at the same streamwise stations in the absence of forcing, figure 6. At the upstream station, $X = 4$, the highest number of small eddies, $N_{max} = 10$, is found around the cores of the ribs and is greater by a factor of 2.5 than the value for the natural case. The value found at the downstream station is $N_{max} = 70$, so the forcing has increased the maximum number of small eddies by about 50% compared with the unforced case (figure 6*b*).

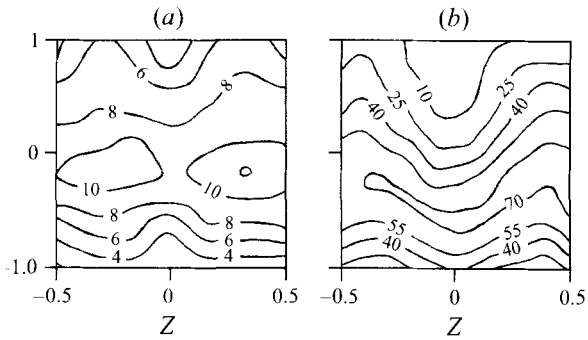

FIGURE 19. Contours of constant N in the (Y,Z)-plane for subharmonic forcing. (*a*) $X = 4$; (*b*) $X = 8$.

6.3. *Effects of other types of forcing*

It is a bit surprising to find that a two-dimensional forcing can have such a strong effect on the generation of small scales. This finding might help in understanding the production mechanism of fine scales, an issue which still remains unsettled. Many features associated with small-scale generation have been observed. For example, the Reynolds number needs to reach a certain level. The initial disturbance level also plays a role (Breidenthal 1981). During the transition, the small-scale turbulence is first found in the core of the newly merged spanwise vortices and in the plane containing the streamwise vortices (Huang & Ho 1987, Moser & Rogers 1992).

An attempt to control the small-scale population by forcing the streamwise vortices was made by placing small passive protrusions at the trailing edge of the splitter plate. The spanwise separation of these protrusions was the same as the spanwise wavelength of the streamwise vortices (Lasheras, Cho & Maxworthy 1986). We could not find any increase in the fine-scale eddy population. We also tried active forcing of the streamwise vortices by replacing the passive protrusions with piezoelectric actuators. The driving frequency was the same as the most preferred frequency, f_p. Again, no effect on the small-scale population was observed.

A recent paper discussing the generation mechanism of small turbulence (Schoppa, Hussian & Metcalfe 1995) could explain the effectiveness of high-level two-dimensional forcing. They suggested that the outburst of small scales is caused by an instability associated with the core of the spanwise structures and that streamwise vortices do not play a role in this process. The instability is related to the amplification of the non-uniform core size and the meridional flow within these structures. The strong two-dimensional perturbation changes the vorticity distribution of the spanwise structures. The core instability could be modified and hence change the small-scale population.

7. Brief summary

During the past two decades, the efforts invested in examining the properties of, and in manipulating, coherent structures have led to major advances in turbulence research. At the same time, experimental tools such as instrumentation and signal-processing techniques, have been significantly improved. Equipped with the concept of coherent structures and the advanced experimental methods, we studied the small-scale turbulence from a perspective different from the traditional statistical approach.

A dissipation microscale has been identified and a control technique of generating small-scale turbulence has been applied in this investigation.

The peak–valley-counting (PVC) technique identifies the local maxima and minima of the velocity fluctuations. Both the velocity extrema values and their instants of occurrence are registered. Based on the magnitude and phase information of fine-scale turbulence, the distribution of the small scales in relation to the large eddies is examined. The small-scale population increases rapidly in the transition region, $X = 4$ to 8. They are concentrated inside the core, in the region with the highest velocity shear.

A pronounced peak was found in the histogram of the length of time between the velocity extrema, which implies that small scales have a preferred length scale. Furthermore, this length scale is almost constant within the velocity shear region. The most interesting feature is that this microscale coincides with the wavelength of the dissipation-spectrum peak. In other words, *this microscale characterizes the typical eddy size which produces most of the viscous dissipation.*

The quantity, $[u_{max} - u_{min}]/\Delta x = \Delta u/\Delta x$, is a measure of the stretching or compression rate produced by small scales. The histogram of this quantity also has a clear peak. We have found that the peak value of $\Delta u/\Delta x$ equals the global strain rate, $\Delta u/\Lambda_0$.

The spanwise forcing technique (Ho & Huang 1982) has been found to be very effective in controlling the evolution of the spanwise structures. The spanwise forcing method, in fact, is also an effective control technique for enhancing the production of fine-scale turbulence in the transition region. However, the forcing level needs to be above a certain threshold and the small-scale population is a function of the forcing amplitude until it reaches a limiting value. Along the streamwise direction, beyond the zone of influence of the forcing, the small-scale populations of the forced and the unforced mixing layers approach the same asymptotic state.

This work is supported by a contract from the Office of Naval Research.

REFERENCES

Bell, J. H. & Mehta, R. D. 1992 Measurements of the streamwise vortical structures in a plane mixing layer. *J. Fluid Mech.* **239**, 213–248.

Bernal, L. P. & Roshko, A. 1986 Streamwise vortex structure in plane mixing layers. *J. Fluid Mech.* **170**, 499–525.

Breidenthal, R. 1981 Structure in turbulent mixing layers and wakes using a chemical reaction. *J. Fluid Mech.* **109**, 1–24.

Brown, G. L. & Roshko, A. 1974 On density effects and large structure in turbulent mixing layer. *J. Fluid Mech.* **64**, 775–816.

Crow, S. C. & Champagne, F. H. 1971 Orderly structure in jet turbulence. *J. Fluid Mech.* **48**, 547–591.

Foss, J. K. 1994 Small-scale turbulence in a plane mixing layer. PhD thesis, University of Southern California.

Ho, C. M. & Gutmark, E. 1987 Vortex induction and mass entrainment in a small-aspect-ratio elliptic jet. *J. Fluid Mech.* **179**, 383–405.

Ho, C. M. & Huang, L. S. 1982 Subharmonics and vortex merging in mixing layers. *J. Fluid Mech.* **119**, 443–473.

Ho, C. M. & Huerre, P. 1984 Perturbed free shear layers. *Ann. Rev. Fluid Mech.* **16**, 365–424.

Ho, C.M. & Zohar, Y. 1996 The dissipation length scale of turbulent shear flows. (in preparation).

Ho, C. M., Zohar, Y., Foss, J. K. & Buell, J. C. 1991 Phase decorrelation of coherent structures in a free shear layer. *J. Fluid Mech.* **230**, 319–337.

HSIAO, F. B. 1985 Small-scale transition and preferred mode in an initially laminar plane jet. PhD thesis, University of Southern California.

HUANG, L. S. 1985 Small-scale transition in a two-dimensional mixing layer. PhD thesis, University of Southern California.

HUANG, L. S. & HO, C. M. 1990 Small-scale transition in a plane mixing layer. *J. Fluid Mech.* **210**, 475–500.

JIMENEZ, J., MARTINEZ-VAL, R. & REBOLLO, M. 1979 On the origin and evolution of three-dimensional effects in the mixing layer. Internal Rep. DA-ERO 79-G-079, Univ. Politec., Madrid.

KONRAD, J. H. 1976 An experimental investigation of mixing in two-dimensional turbulent shear flows with applications to diffusion-limited chemical reactions. Tech. Rep. Internal Rep. CIT-8-PU, Calif. Inst. Technol.

LASHERAS, J. C., CHO, J. S. & MAXWORTHY, T. 1986 On the origin and evolution of streamwise vortex structures in a plane free shear layer. *J. Fluid Mech.* **172**, 231–258.

LIU, J. T. C. 1981 Interactions between large-scale coherent structures and fine-grained turbulence in free shear flows. In *Transition and Turbulence* (ed. R. E. Meyer). Academic.

MONKEWITZ, P. A. & HUERRE, P. 1982 The influence of the velocity ratio on the spatial instability of mixing layers. *Phys. Fluids* **25**, 1137–1143.

MOSER, R. D. & ROGERS, M. M. 1993 The three-dimensional evolution of a plane mixing layer: pairing and transition to turbulence. *J. Fluid Mech.* **247**, 275–320.

NYGAARD, K. J. & GLEZER, A. 1991 Evolution of streamwise vortices and generation of small-scale motion in a plane shear layer. *J. Fluid Mech.* **231**, 257–301.

OSTER, D. & WYGNANSKI, I. 1982 The forced mixing layer between parallel streams. *J. Fluid Mech.* **123**, 91–130.

PIERREHUMBERT, R. T. & WIDNALL, S. E. 1982 The two- and three-dimensional instabilities of a spatially periodic shear layer. *J. Fluid Mech.* **114**, 59–82.

ROGERS, M. M. & MOSER R. D. 1992 The three-dimensional evolution of a plane mixing layer: The Kelvin–Helmholtz rollup. *J. Fluid Mech.* **243**, 183–226.

ROSHKO, A. 1976 Structure of turbulent shear flows: a new look. *AIAA J.* **14**, 1349–1357.

SCHOPPA, W., HUSSIAN, F. & METCALFE, R. W. 1995 A new mechanism of small-scale transition in a plane mixing layer: core dynamics of spanwise vortices. *J. Fluid Mech.* **298**, 23–80.

TENNEKES, H. & LUMLEY, J. L. 1972 *A First Course of Turbulence.* MIT Press.

WINANT, C. D. & BROWAND, F. K. 1974 Vortex pairing: the mechanism of turbulent mixing layer growth at moderate Reynolds number. *J. Fluid Mech.* **63**, 237–255.

WYGNANSKI, I. & FIEDLER, H. E. 1970 The two-dimensional mixing layer. *J. Fluid Mech.* **41**, 327–361.

WYGNANSKI, I. & PETERSEN, R. A. 1987 Coherent motion in excited free shear flows. *AIAA J.* **25**, 201–213.

WYNGAARD, J. C. 1968 Measurement of small-scale turbulence structure with hot wires. *J. Sci. Instrum.* **1**, 1105–1108.

ZHANG, Y. Q., HO, C. M. & MONKEWITZ, P. A. 1985 The mixing layer forced by fundamental and subharmonic. In *IUTAM Symposium on Laminar-Turbulent Transition, Novosibirsk* (ed. V. Kozlov), pp. 385–395. Springer.

ZOHAR, Y. 1990 Fine scale mixing in a plane mixing layer. PhD thesis, University of Southern California.

ZOHAR, Y., HO, C. M., MOSER, R. P. & BUELL, J. C. 1990 Length scales and dissipation of fine eddies in a mixing layer. In *Studying Turbulence Using Numerical Simulation III* (ed. P. Moin, W. C. Reynolds & J. Kim), pp. 225–234. NASA.